THE JOURNAL OF BIOLOGICAL CHEMISTRY
Vol. 280, No. 11, Issue of March 18, pp. 10378–10387, 2005
Printed in U.S.A.

A Molecular Mechanism for Lipopolysaccharide Protection of Gram-negative Bacteria from Antimicrobial Peptides*

Received for publication, November 15, 2004, and in revised form, December 20, 2004
Published, JBC Papers in Press, January 4, 2005, DOI 10.1074/jbc.M412865200

Niv Papo and Yechiel Shai‡

From the Department of Biological Chemistry, Weizmann Institute of Science, Rehovot 76100, Israel

Cationic antimicrobial peptides serve as the first chemical barrier between all organisms and microbes. One of their main targets is the cytoplasmic membrane of the microorganisms. However, it is not yet clear why some peptides are active against one particular bacterial strain but not against others. Recent studies have suggested that the lipopolysaccharide (LPS) outer membrane is the first protective layer that actually controls peptide binding and insertion into Gram-negative bacteria. In order to shed light on these interactions, we synthesized and investigated a 12-mer amphipathic α-helical antimicrobial peptide (K_5L_7) and its diastereomer (4D-K_5L_7) (containing four D-amino acids). Interestingly, although both peptides strongly bind LPS bilayers and depolarize bacterial cytoplasmic membranes, only the diastereomer kills Gram-negative bacteria. Attenuated total reflectance Fourier transform infrared, CD, and surface plasmon resonance spectroscopies revealed that only the diastereomer penetrates the LPS layer. In contrast, K_5L_7 binds cooperatively to the polysaccharide chain and the outer phosphate groups. As a result, the self-associated K_5L_7 is unable to traverse through the tightly packed LPS molecules, revealed by epifluorescence studies with LPS giant unilamellar vesicles. The difference in the peptides' modes of binding is further demonstrated by the ability of the diastereomer to induce LPS miscellization, as shown by transmission electron microscopy. In addition to increasing our understanding of the molecular basis of the protection of bacteria by LPS, this study presents a potential strategy to overcome resistance by LPS, and it should help in the design of antimicrobial peptides for future therapeutic purposes.

Cationic antimicrobial peptides are gene-encoded polypeptides, which serve as essential components of the innate immune system of all species, including humans (1–4). These peptides are mobilized shortly after microbial infection and act rapidly to neutralize a broad range of microbes. This quick response is crucial, because activation of pathogen-specific immune responses occurs slowly relative to the potential kinetics of microbial proliferation (1, 5) (for a recent review, see Ref. 6). At present, hundreds of these peptides have been isolated from different biological sources (see list on the World Wide Web at www.bbcm.univ. trieste.it/~tossi/pag1.htm), some of which were subjected to mode of action studies. These studies indicate that the bacterial cytoplasmic membrane is one of the main targets for many of these peptides (7–12). Interestingly, however, some antimicrobial peptides, which bind, permeate, and depolarize efficiently bacterial membranes, have limited activity on intact bacteria (11, 13–15). For example, insect cecropins are in practice active only on Gram-positive bacteria (16), compared with magainins (17), dermaseptins (18), and many others, which are active on both Gram-negative and Gram-positive bacteria. Other examples include cathelicidins, protegrins, defensins, and temporins (16–21).

For most antimicrobial peptides that are not active against Gram-negative bacteria, the outer membrane is believed to be a major barrier (10, 16, 22–29). However, the details of the interactions of the peptides with these membranes are still not fully known (23, 30–32). The outer membrane of Gram-negative bacteria mostly contains (>90%) the glycolipid lipopolysaccharides (LPS)[1] on its surface, the structure of which is not well known (23, 33–38). LPS is generally thought to be a protective wall, rendering bacteria resistant to a variety of host defense molecules (24). Indeed, LPS allows the traverse of hydrophobic molecules at about 1–2% of the rates observed with typical phospholipid bilayers (36, 39). LPS has two potential barriers; one is hydrophilic (provided by the oligosaccharide core, which is densely packed (33)), and the other is hydrophobic (provided by the hydrocarbon chain region, which contains six fatty acids per molecule (32, 40)).

In order to address the question as to whether bacterial LPS is responsible for the different susceptibilities of Gram-negative bacteria toward a certain peptide, we synthesized and investigated a 12-mer amphipathic peptide (K_5L_7) and its diastereomeric counterpart (containing 33% D-residues). These peptides were selected because they have the same amino acid composition, but the incorporation of D-amino acids should affect the structure and organization of the diastereomer. Importantly, we found that the diastereomer is highly active on Gram-negative bacteria, whereas the parental peptide is not.

The peptides were investigated, by using various biophysical methods, for their interaction with LPS in the form of bilayers, small (SUVs), large (LUVs) and giant unillamelar vesicles (GUVs). These include fluorescence spectroscopy, Fourier transform infrared spectroscopy (FTIR), surface plas-

* This work was supported by the Israel Science Foundation. The costs of publication of this article were defrayed in part by the payment of page charges. This article must therefore be hereby marked "*advertisement*" in accordance with 18 U.S.C. Section 1734 solely to indicate this fact.

‡ The Harold S. and Harriet B. Brady Professorial Chair in Cancer Research. To whom correspondence should be addressed. Tel.: 972-8-9342711; Fax: 972-8-9344112; E-mail: Yechiel.Shai@weizmann.ac.il.

[1] The abbreviations used are: LPS, lipopolysaccharide(s); ATR-FTIR, attenuated total reflectance Fourier transform infrared; Fmoc, *N*-(9-fluorenyl)methoxycarbonyl; diS-C_3-5, 3,3′-diethylthiodicarbocyanine iodode; hRBC, human red blood cell; SUV, small unilamellar vesicle; LUV, large unilamellar vesicle; GUV, giant unilamellar vesicle; MIC, minimal inhibitory concentration; PBS, phosphate-buffered saline; PE, *E. coli* phosphatidylethanolamine; PG, egg phosphatidylglycerol; Rho, tetramethylrhodamine; RP-HPLC, reverse phase high performance liquid chromatography; RU, response unit(s); SPR, surface plasmon resonance; aa, amino acid(s).

mon resonance (SPR) spectroscopy, epifluorescence, and transmission electron microscopies. The observed biophysical data were complemented by biological assays, both providing information about the dependence of the antimicrobial activity on the peptides' hydrophobicity, structure, and oligomeric state. Based on the data collected, we propose a molecular mechanism for the peptide-LPS interactions that allows the peptides to traverse or prevents them from transversing the LPS layer and the target inner membrane.

EXPERIMENTAL PROCEDURES

Materials

Rink amide 4-methyl benzhydrylamine resin and Fmoc aa were obtained from Calbiochem-Novabiochem AG (Switzerland). Other reagents used for peptide synthesis included trifluoroacetic acid (Sigma), piperidine (Merck), *N*,*N*-diisopropylethylamine (Sigma), *N*-hydroxybenzotriazole hydrate (Aldrich), 2-(1H-benzotriazole-1-yl)-1,1,3,3-tetramethyluronium hexafluorophosphate, and dimethylformamide (peptide synthesis grade; Biolab). Trypsin, proteinase-K, egg phosphatidylglycerol (PG), phosphatidylethanolamine (PE) (Type V, from *Escherichia coli*), LPS (from *E. coli* 055:B5), *N*-octyl β-D-glucopyranoside, and bovine serum albumin were purchased from Sigma. 3,3′-diethylthio-dicarbocyanine iodide (diS-C_3-5) and Rho-PE were obtained from Molecular Probes, Inc. (Eugene, OR). All other reagents were of analytical grade. Buffers were prepared in double glass-distilled water.

Peptide Synthesis and Purification

Peptides were synthesized by an Fmoc solid phase method on Rink amide 4-methyl benzhydrylamine resin, using an ABI 433A automatic peptide synthesizer. Cleavage of the peptides from the MBHA resin resulted in C terminus-amidated peptides. The peptides were purified by RP-HPLC on a C_{18} reverse phase Bio-Rad semipreparative column (250 × 10 mm, 300-Å pore size, 5-cm particle size). The column was eluted in 40 min, using a linear gradient of 20–60% acetonitrile in water, containing 0.05% trifluoroacetic acid (v/v), at a flow rate of 1.8 ml/min. The purified peptides were further subjected to amino acid analysis and electrospray mass spectroscopy to confirm their compositions and molecular weights.

Preparation of SUVs, LUVs, and GUVs

Multilamellar vesicles were first made using the following procedure. PE/PG (7:3, w/w) and LPS were dissolved in chloroform/methanol (2:1), and after the solvent was removed they were suspended in buffer (10 mg/ml), heated to 60 °C (only in LPS), and vortexed. The different types of vesicles were made as follows. (i) For BIAcore experiments, SUVs were prepared by sonication of LPS multilamellar vesicles as described previously (37, 41). (ii) For membrane depolarization and electron microscopy experiments, LUVs were prepared using a procedure described elsewhere (36). Briefly, PE/PG multilamellar vesicles were extruded 15 times through two stacked 100-nm polycarbonate filters, whereas for LPS, the extrusions were performed at 60 °C (34). (iii) For epifluorescence experiments, PE/PG/PE-Rho (7/3/0.1, w/w/w) or LPS/PE-Rho (10/0.1, w/w) GUVs were prepared using a procedure described previously (42). Briefly, the lipid films were dissolved in chloroform (0.1 M), and 20 μl of this solution was added to a 50-ml round-bottomed flask containing 980 μl of chloroform and 150 μl of methanol. The aqueous phase (7 ml of PBS) was then cautiously added along the flask walls. The organic solvent was removed in a rotary evaporator under reduced pressure at 40 °C and 40 rpm. The resulting aqueous solution contained GUVs in a high concentration.

Both SUVs and LUVs were visualized using a JEOL JEM 100B electron microscope (Japan Electron Optics Laboratory Co., Tokyo, Japan) as follows. A drop of the vesicles was deposited on a carbon-coated grid and negatively stained with uranyl acetate. Examination of the grids showed that the vesicles were unilamellar with an average diameter of 20–50 nm with SUV and 100 nm with LUV. GUVs were visualized using an Olympus FV500 confocal laser-scanning microscope. Examination of the samples showed that the vesicles were unilamellar with an average diameter of 10–20 μm. Phospholipid concentrations in SUVs, LUVs, and GUVs were measured by phosphate analysis (34).

Antibacterial Activity of the Peptides and Their Stability toward Enzymatic Degradation

The antibacterial activity of the peptides was examined in sterile 96-well plates (Nunc F96 microtiter plates) in a final volume of 100 μl as follows. Aliquots (50 μl) of a suspension containing bacteria (midlog phase) at a concentration of 10^6 colony-forming units/ml in culture medium (LB medium) were added to 50 μl of water containing the peptide in serial 2-fold dilutions in water. Inhibition of growth was determined by measuring the absorbance at 600 nm with a Microplate autoreader El309 (Bio-tek Instruments) after an incubation of 18–20 h at 37 °C. Antibacterial activities were expressed as the minimal inhibitory concentration (MIC), the concentration at which 100% inhibition of growth was observed after 18–20 h of incubation. In order to test the antibacterial activity of the peptide in serum, a similar protocol was used but with the peptides dissolved in 30% human blood serum. The Gram-negative bacterial strains used were *E. coli* ATCC 25922, *Shigella sonnei* ATCC 25931 and *Salmonella choleraesuis* ATCC 14028.

For stability studies, trypsin or proteinase-K (10 μg/ml in PBS) was added to a solution of the peptides in PBS (1 μM), and the reaction was monitored by using RP-HPLC and electrospray mass spectroscopy, as described before.

Kinetics of Killing

The *in vitro* bactericidal potency (time-kill curve) of the peptides toward the Gram-negative bacteria *Escherichia coli* ATCC 25922 was also measured. In this assay, about 10^6 colony-forming units/ml of bacteria in culture medium were separately incubated in the presence of the peptides (in their MIC values) for 1, 2, 4, 6, 8, 12, and 18 h. Aliquots of bacterial culture were plated on agar medium, and colonies were counted after incubation for 16 h at 37 °C.

Hemolysis of Human Red Blood Cells (hRBCs)

Fresh hRBCs were rinsed three times with PBS (35 mM phosphate buffer, 0.15 M NaCl, pH 7.3) by centrifugation for 10 min at 800 × *g* and resuspended in PBS. Peptides dissolved in PBS were then added to 50 μl of the stock hRBC solution in PBS to make a final volume of 100 μl (final erythrocyte concentration, 4% (v/v)). The resulting suspension was incubated with agitation for 60 min at 37 °C. The samples were then centrifuged at 800 × *g* for 10 min. By measuring the absorbance of the supernatant at 540 nm, we monitored the release of hemoglobin. Controls for zero hemolysis (blank) and 100% hemolysis consisted of hRBCs suspended in PBS and 1% Triton, respectively.

Increase in Membrane Permeability Induced by the Peptides

Membrane destabilization, which results in the collapse of the diffusion potential, was detected fluorimetrically as described previously (43–45). Briefly, a PE/PG or LPS LUV suspension, prepared in "K^+ buffer" (50 mM K_2SO_4/25 mM HEPES-sulfate, pH 6.8), was added to an isotonic K^+-free buffer (50 mM Na_2SO_4, 25 mM HEPES-sulfate, pH 6.8), and the dye diS-C_3-5 was then added. The subsequent addition of valinomycin created a negative diffusion potential inside the vesicles by the selective efflux of K^+ ions, which resulted in a quenching of the dye's fluorescence ($\Delta\Psi = -142$ mV). Peptide-induced membrane permeation for all of the ions in the solution caused a dissipation of the diffusion potential, manifested by an increase in fluorescence. Fluorescence was monitored using excitation and emission wavelengths at 620 and 670 nm, respectively. The percentage of fluorescence recovery, F_t, was defined by the equation,

$$Ft = ((I_t - I_o)/(I_f - I_o))100\% \quad \text{(Eq. 1)}$$

where I_t represents the fluorescence observed after the addition of a peptide at time t, I_o is the fluorescence after the addition of valinomycin, and I_f is total fluorescence before adding valinomycin.

Transmembrane Potential Depolarization Assay with Bacteria

The depolarization assay was conducted with intact Gram-negative bacteria and bacterial spheroplasts using a protocol similar to what was reported before (25) and for mutated bacteria (46).

Intact Bacteria—E. coli ATCC 25922 bacteria were grown at 37 °C with agitation until reaching a midlog phase (A_{600} = 0.4). The bacteria were centrifuged and washed once with buffer (20 mM glucose, 5 mM HEPES, pH 7.3), and resuspended to an A_{600} of 0.05 in a similar buffer containing 0.1 M KCl. The bacteria (in the same concentrations as in the biological activity assay) were then incubated with 1 μM diS-C_3-5 until a stable reduction of fluorescence was achieved (approximately after 60 min), indicating that the dye was incorporated into the bacterial membrane. The peptides were then added from a water stock solution (1 mg/ml) and dissolved in the KCl buffer to achieve the desired concentration (0.1–5-fold the MIC). Membrane depolarization was monitored by observing the change in the intensity of the fluorescence emission of the membrane potential-sensitive dye diS-C_3-5 (excitation wavelength

λ_{ex} = 622 nm, emission wavelength λ_{em} = 670 nm), after the addition of different concentrations of the peptide.

Bacterial Spheroplasts—Spheroplasts of *E. coli* ATCC 25922 (LPS and peptidoglycan-free bacteria (47)) were prepared by the osmotic shock procedure as follows. First, the cells from cultures grown to A_{600} = 0.8 were harvested by centrifugation and washed twice with 10 mM Tris/H_2SO_4, 25% sucrose, pH 7.5. Next, the cells were resuspended in a washing buffer containing 1 mM EDTA. After a 10-min incubation at 20 °C with rotary mixing, the cells were collected by centrifugation and resuspended immediately in water (4 °C). After a 10-min incubation at 4 °C with rotary mixing, the spheroplasts were collected by centrifugation. The spheroplasts were then resuspended to A_{600} = 0.05 in a buffer containing 20 mM glucose, 5 mM HEPES, 1 M KCl, pH 7.3. Further treatment was done exactly as described for the intact bacteria.

ATR-FTIR Measurements

This technique was used to obtain information on the influence of the peptides on the phosphate groups and on the acyl chains of LPS as well as the influence of LPS on the secondary structure of the peptides. Spectra were obtained with a Bruker equinox 55 FTIR spectrometer equipped with a deuterated triglyceride sulfate detector and coupled to an ATR device as described previously (48). Briefly, a mixture of LPS (0.5 mg) alone or with peptide (~20 μg) was deposited on a ZnSe horizontal ATR prism (80 × 7 mm). Lipid/peptide mixtures were prepared by dissolving them together in a 1:2 MeOH/CH_2Cl_2 mixture and drying under a stream of dry nitrogen while moving a Teflon bar back and forth along the ZnSe prism. Spectra were recorded, and the respective pure phospholipid spectra were subtracted to yield the difference spectra. The background for each spectrum was a clean ZnSe prism. Hydration of the sample was achieved by introducing excess deuterium oxide (^2H_2O) into a chamber placed on top of the ZnSe prism in the ATR casting and incubating for 2 h before acquisition of the spectra. H/D exchange was considered complete after total shift of the amide II band. Any contribution of ^2H_2O vapor to the absorbance spectra near the amide I peak region was eliminated by subtracting the spectra of pure lipids equilibrated with ^2H_2O under the same conditions.

ATR-FTIR Data Analysis

Prior to curve fitting, a straight base line passing through the ordinates at 1700 and 1600 cm^{-1} was subtracted. To resolve overlapping bands, the spectra were processed using PEAKFIT™ (Jandel Scientific, San Rafael, CA) software. Second derivative spectra were calculated to identify the positions of the component bands in the spectra. These wave numbers were used as initial parameters for curve fitting with Gaussian component peaks. Position, band widths, and amplitudes of the peaks were varied until (i) the resulting bands shifted by no more than 2 cm^{-1} from the initial parameters, (ii) all of the peaks had reasonable half-widths (<20–25 cm^{-1}), and (iii) good agreement between the calculated sum of all of the components and the experimental spectra was achieved ($r^2 > 0.99$). The relative contents of the different secondary structure elements were estimated by dividing the areas of individual peaks, assigned to a specific secondary structure, by the whole area of the resulting amide I band. The results of three independent experiments were averaged.

The interactions of the peptides with LPS head groups were studied by monitoring the antisymmetric stretching vibration of the negatively charged phosphate groups, $\nu_{as}(PO_2)$, ranging from 1220 to 1260 cm^{-1} (38, 49). The interaction of the peptides with LPS acyl chains was studied by analyzing the polarized ATR-FTIR spectra as described previously (50, 51).

CD Spectroscopy

The CD spectra of the peptides were measured with a Jasco J-500A spectropolarimeter after calibrating the instrument with (+)-10-camphorsulfonic acid. The spectra were scanned at 25 °C in a capped, quartz optical cell with a 0.5-mm path length. Spectra were obtained at wavelengths of 190–250 nm. Eight scans were taken for each peptide at a scan rate of 20 nm/min. Mean residue ellipticities were expressed as [θ] (degrees·cm^2/dmol). The peptides were scanned at 25 μM in the presence of 0.1% (~0.22 mM) LPS. Fractional helicity was calculated from the dichroic minimum at 222 nm, as described previously (52, 53). The $\theta_{222}/\theta_{208}$ ratio was calculated in order to estimate helix-helix interactions (54).

LPS Binding Obtained by SPR

Binding of the peptides to LPS bilayers (using L1 chip) was assessed with a BIAcore 3000 analytical system (Biacore, Uppsala, Sweden). This technology uses SPR to study biomolecular interaction in real time. A similar approach was used to study LPS interaction with the antimicrobial peptide protegrin-1 (using an HPA sensor chip, which creates LPS monolayers) (55). The L1 sensor chip is composed of hydrophobic aliphatic chains that contain exposed polar head groups. Thus, when in contact with vesicles, a lipid bilayer is formed. We performed the protocol described by Mozsolits *et al.* (56). Briefly, LPS SUVs (80 μl, 0.5 mM) were applied to the L1 chip surface at a low flow rate (2 μl/min). To remove any multilamellar structures from the lipid surface, we increased the flow rate to 50 μl/min, which resulted in a stable base line corresponding to the lipid bilayer linked to the chip surface. The negative control bovine serum albumin was injected (25 μl; 0.1 mg/μl in PBS) to confirm complete coverage of the nonspecific binding sites. The bilayer linked to the chip surface was then used as a model cell membrane surface to study the peptide-membrane binding. Peptide solutions (40-μl solution of 0.39–12.5 μM peptide) were injected on the lipid surface at a flow rate of 5 μl/min. Buffer (pH 7.0) alone was then replaced by the peptide solution for 30 min to allow peptide dissociation. Peptide solutions were either prepared in 20 mM Hepes, 10 mM EDTA, 90 mM NaCl, pH 7.0, or in 20 mM Hepes, 0.5 mM $MgCl_2$, 90 mM NaCl, pH 7.0 (34). The SPR, which is expressed in resonance units (RU), detects changes in the reflective index of the surface layer of peptides and lipids in contact with the sensor chip. A sensogram was obtained by plotting the RU against time. The peptide-lipid binding event was analyzed from a series of sensograms collected at seven different peptide concentrations.

We used a kinetic model to describe the peptide-lipid interactions. More specifically, the sensograms for each peptide-lipid bilayer interaction were analyzed by curve fitting using numerical integration analysis (57). The BIAevaluation software offers different reaction models to perform complete kinetic analyses of the peptide sensograms. One curve-fitting algorithm (the two-state reaction model) was chosen on the basis of what was known about the possible binding mechanisms of lytic peptides (58). The data were fitted globally by simultaneously fitting the peptide sensograms obtained at seven different concentrations. The two-state reaction model was applied to each data set. This model describes two reaction steps (56), which, in terms of peptide-lipid interaction, corresponds to the following,

$$P + L \underset{k_{d1}}{\overset{k_{a1}}{\rightleftharpoons}} PL \underset{k_{d2}}{\overset{k_{a2}}{\rightleftharpoons}} PL^*$$

REACTION 1

where, in the first step, peptide (P) binds to lipids (L) to give PL, which is changed to PL* in the second step. PL* cannot dissociate directly to P + L and may correspond to partial insertion of the peptide into the lipid bilayer. The corresponding differential rate equations for this reaction model are represented by the following,

$$dRU_1/dt = k_{a1} \times C_A \times (RU_{max} - RU_1 - RU_2) - k_{d1} \times RU_1 - k_{a2} \times RU_1 + k_{d2} \times RU_2 \quad \text{(Eq. 2)}$$

$$dRU_2/dt = k_{a2} \times RU_1 - k_{d2} \times RU_2 \quad \text{(Eq. 3)}$$

where RU_1 and RU_2 are the response units for the first and second steps, respectively, C_A is the peptide concentration, RU_{max} is the maximal response unit, and k_{a1}, k_{d1}, k_{a2}, and k_{d2} are the association and dissociation rate constants for the first and second steps, respectively. Whereas k_{a1} has 1/(M× s) units, k_{d1}, k_{a2}, and k_{a2} have 1/s units. Thus, the combined affinity constant for all of the process, K, has M^{-1} units. We also described the relationship between the maximal binding response for each peptide concentration (RU_{max}) and the peptide concentration (C) to evaluate cooperativity in binding.

Epifluorescence Microscopy

For epifluorescence microscopy studies (59, 60), the fluorescent dye Rho-PE was dissolved with PE/PG (7:3, w/w) and LPS in chloroform/methanol in molar ratios [PE/PG]/[Rho-PE] or [LPS]/[Rho-PE] of 100:1 (38). GUVs were prepared (as described above), and images were obtained using an Olympus FV500 confocal laser-scanning microscope. Liquid-condensed (LC) domains and liquid-expanded (LE) domains were distinguished. Using the fluorescent dye Rho-PE, the LE domains appear red, and the LC domains dark (38). The setting of the photomultipliers (gain and black level) was constant for the series of images. Care was taken that any photobleaching did not compromise the interpretation, and laser irradiation and other illumination were prevented

TABLE I
Designations, sequences, retention times, percentages of enzymatic degradation, minimal inhibitory concentrations, and hemolytic activities of the peptides

Peptide designation	Sequence[a]	RP-HPLC retention time[b]	Enzymatic degradation[c]	*E. coli* ATCC 25922	*S. sonnei* 0ATCC 25931	*S. choleraesuis* ATCC 14028	Hemolysis at 100 μM
		min	%	μM	μM	μM	%
K_5L_7	KLLLKLKLKLLK-NH_2	21.3	100	>100 (>100)[d]	>100 (>100)	>100 (>100)	80
4D-K_5L_7	KL**LL**KLK**L**K**L**LK-NH_2	17.3	6	5 (8)	4 (8)	8 (8)	0

[a] Underlined and boldface amino acids are D-enantiomers. All the peptides are amidated at their C terminus.
[b] A C_{18} reverse phase analytical column was used. The peptides were eluted in 40 min, using a linear gradient of 20–60% acetonitrile in water, both containing 0.05% trifluoroacetic acid (v/v).
[c] Peptides were treated for 2 h with trypsin or proteinase-K.
[d] The activities of the peptides in the presence of serum are shown in parentheses.

between acquisitions. The confocal images were obtained at a 12-bit resolution.

Examination of LUV Damage by Electron Microscopy

Samples containing LPS LUVs were incubated with (i) 10 μM K_5L_7 and (ii) 3 and 5 μM of 4D-K_5L_7 (at which the diastereomer exhibited 50 and 80% of its maximal activity in the membrane permeability study). A drop containing the vesicles was deposited onto a carbon-coated grid and negatively stained with phosphotungstic acid (2%), pH 6.8. The grids were examined using a JEOL JEM 100B electron microscope (Japan Electron Optics Laboratory Co., Tokyo, Japan).

RESULTS

In order to correlate antimicrobial activity with binding and permeating by the bacterial LPS, we used two antimicrobial peptides; one is highly active against Gram-negative bacteria but is not hemolytic, and the other is highly hemolytic but inactive against the same bacteria. The sequence of the peptides, their biological activity, and RP-HPLC retention times are given in Table I. Both peptides have the same amino acid composition, but one contains four Leu as D-enantiomers, which rendered it significantly less hydrophobic compared with the parental peptides (shorter retention time). Because of their similar composition, the difference in their retention times is probably due to differences in their structures upon their interaction with the hydrophobic C_{18} chain of the RP-HPLC column, which can be considered as a simple model for lipid environment (61). The peptides were studied for their structure and mode of action with intact bacteria, bacteria spheroplasts, phospholipid membranes, and LPS membrane systems (including SUVs, LUVs, GUVs, bilayers, and multibilayers), by using fluorescence, CD, and FTIR spectroscopy as well as SPR and confocal and electron microscopy.

Antimicrobial Activities of the Peptides in Buffer and Serum and Their Hemolytic Activity—Antibacterial activity was assayed against a representative set of Gram-negative bacteria including *E. coli* ATCC 25922, *S. sonnei* ATCC 25931, and *S. choleraesuis* ATCC 14028. The parental peptide, K_5L_7, was designed to have an amphipathic α-helix structure with one face composed of charged aa and the opposite face composed of hydrophobic aa. Unexpectedly, K_5L_7 was more than 10-fold less active than its diastereomer against all Gram-negative bacteria tested (Table I). Similar results were obtained in the presence of 30% human serum. Furthermore, incorporating D-aa into the peptide's sequence rendered it less susceptible to enzymatic degradation (Table I). Note that, whereas the antimicrobial assay proceeds for 18–20 h at 37 °C, all other assays took place for significantly shorter times (0.5–2 h). We therefore performed time-killing experiments in which we monitored the killing of bacteria as a function of time. The data revealed similar kinetics for the two peptides at their MICs; 90% suppression of bacteria growth was observed 1 h following the addition of 10 μM 4D-K_5L_7 and 100 μM K_5L_7. These results enabled us to correlate between the biological and biophysical assays.

Membrane Depolarization Induced by the Peptides—The ability of the peptides to depolarize the bacterial inner and outer membranes was determined in PE/PG LUVs (62), LPS LUVs, *E. coli* spheroplasts, and intact bacteria, as described previously (25, 46). Briefly, the peptides were mixed at various concentrations with vesicles (or bacterial cells) pretreated with the fluorescent dye, diS-C_3-5, and valinomycin (for vesicles only). The fluorescent dye exhibits decreased fluorescence when it partitions into the membrane. An increase in fluorescence in the presence of a peptide indicates its ability to depolarize the membrane. Fig. 1 shows the dose-dependent dissipation of the transmembrane potential of PE/PG LUVs (*A*), LPS LUVs (*B*), *E. coli* spheroplasts (*C*), and intact cells (*D*). The data revealed that both K_5L_7 and 4D-K_5L_7 induced the depolarization of PE/PG LUVs and *E. coli* spheroplasts to a similar extent, despite the significant difference in their antimicrobial activities (Table I). However, a direct correlation was found between the antimicrobial activity of the peptides and their ability to depolarize LPS LUVs and intact *E. coli* cells. This evidence strongly suggests that the major target of the peptides is the inner membrane, and that their different MIC values are the result of their different abilities to traverse the outer membrane of the LPS, a process described as a self-promoted uptake (63). The incorporation of D-aa into the peptide affected its structure and oligomeric state (see below).

Secondary Structure of the Peptides in LPS Membranes, as Determined by FTIR Spectroscopy—Fourier-transformed infrared spectroscopy (FTIR) is a powerful tool available to obtain information on the mode of interaction of peptides with membranes. The secondary structure components of a peptide in a membrane-bound state can be determined from the wave numbers of the amine I vibration (followed by deconvolution) either before or after deuteration. Here we determined the secondary structure of the peptides bound to LPS after complete deuteration. The amide I region spectra as well as the fitted band components (obtained by deconvolution) of K_5L_7 and 4D-K_5L_7 that are bound to LPS multibilayers are shown in Fig. 2, *A* and *B*, respectively. Assignment of the different secondary structures to the various amide I regions was calculated according to the values taken from others (64, 65) and our previous results (66–68). The assignments and the relative areas of the component peaks are summarized in Table II. The results indicate strong bands typical for α-helical structures at 1650 cm^{-1} and the 3_{10}-helix at 1658 cm^{-1}, for K_5L_7 and 4D-K_5L_7, respectively. In support of this, the amide I region from 1656 to 1670 cm^{-1} is characteristic of a 3_{10}-helix or dynamic/distorted α-helix, as was previously suggested in a study that examined the structural changes in phospholipase A_2 (69). The assignment of the amide I region from 1656 to 1670 cm^{-1} to the dynamic helix is further supported by studies that examined distorted α-helical structures (a_{II}-helices) in bacteriorhodopsin and other proteins (70, 71). Similar structures were reported previously for a model amphipathic α-helical peptide and its diastereomer (25).

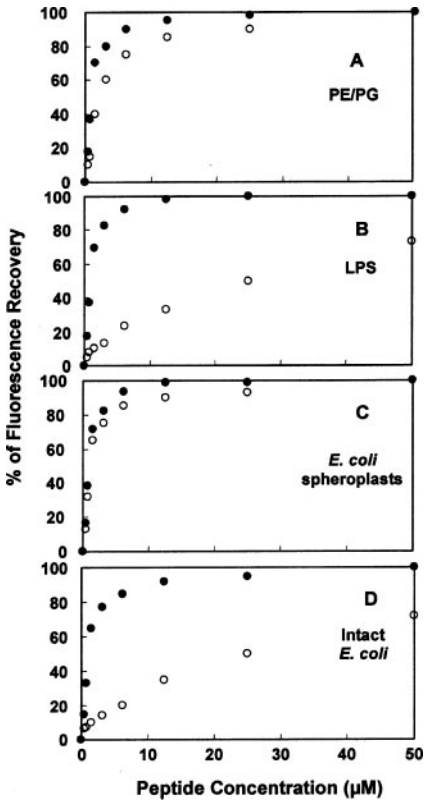

FIG. 1. **Maximal dissipation of the diffusion potential in lipid vesicles (*A* and *B*), membranes of *E. coli* spheroplasts (*C*) and intact *E. coli* cells (*D*).** In the case of vesicles, the peptides were added to isotonic K^+-free buffer containing LUVs composed of PE/PG (*A*) or LPS (*B*), pre-equilibrated with the fluorescent dye diS-C_2-5 and valinomycin. In the case of the spheroplasts (*C*) and intact bacteria (*D*), the peptides were added to bacterial cells that were pre-equilibrated with the fluorescent dye diS-C_2-5 for 60 min. Fluorescence recovery was measured 1–120 min (at 5-min intervals) after the peptides were added and its maxima were recorded. Designations are as follows: K_5L_7 (●) and 4D-K_5L_7 (○).

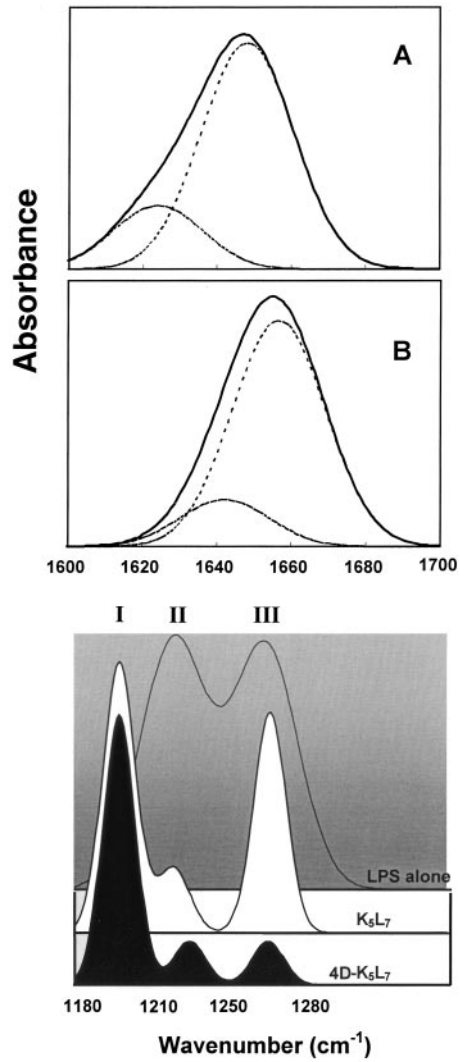

FIG. 2. **FTIR spectra deconvolution of the fully deuterated amide I band (1600–1700 cm^{-1}) of K_5L_7 (*A*) and 4D-K_5L_7 (*B*) peptides in LPS multibilayers.** Second derivatives were calculated to identify the positions of the component bands in the spectra. The component peaks are the result of curve-fitting using a Gaussian line shape. The sums of the fitted components superimpose on the experimental amide I region spectra. *Continuous lines* represent the experimental FTIR spectra; *broken lines* represent the fitted components. *C*, the influence of the different peptides on the head groups of LPS. IR absorbance spectra are shown for LPS multibilayers in the range of the asymmetric stretching vibration of the negatively charged phosphates $\nu_{as}(PO_2)$ for the different peptides. *I* designates the IR band of the peptide; *II* and *III* are the vibrational bands of LPS corresponding to different hydration of the phosphates. A 60:1 lipid/peptide molar ratio was used.

The structure of each peptide did not change when 1:60 and 1:120 peptide/lipid molar ratios were used.

Interaction of the Peptides with Phosphate Groups and Acyl Chains in LPS—The antisymmetric stretching vibration of the negatively charged phosphate ν_{as} (PO_2^-) was used to indicate an interaction of the peptides with the backbone region of LPS. In the range of this vibration, namely 1280–1230 cm^{-1}, a drastic change in the band shape can be seen. More specifically, the band is split into two vibrational bands, indicating different hydration states (Fig. 2*C*, bands II and III), with the band at the higher wave number (band III) representing a lower hydration (38, 40). The addition of both K_5L_7 and 4D- K_5L_7 led to a strong reduction of the band intensities, indicating immobilization of the phosphate groups. Interestingly, the binding of K_5L_7 led to a reduction of only band II, whereas the binding of 4D-K_5L_7 reduced both bands (II and III). This is probably due to the inability of the aggregated all-L-peptide (see below) to reach the less exposed inner phosphate (band III).

The ability of the peptides to disrupt lipid acyl chains was evaluated by using polarized ATR-FTIR spectroscopy. The symmetric ($\upsilon_{sym}(CH_2) \approx 2853$ cm^{-1}) and the antisymmetric ($\upsilon_{sym}(CH_2) \approx 2922$ cm^{-1}) vibrations of lipid methylene C–H bonds are perpendicular to the molecular axis of a fully extended hydrocarbon chain. Thus, measuring the dichroism of infrared light absorbance can reveal the order of the membrane sample relative to the prism surface. The effect of the peptides on the acyl chain order was estimated by comparing the CH_2 stretching dichroic ratio of LPS phospholipid multibilayers alone with that obtained with LPS-bound peptides. The calculated values (*R*), based on the antisymmetric vibrations, were higher for 4D-K_5L_7 compared with K_5L_7, indicating that the diastereomer had a stronger effect on the acyl chain order of LPS (Table II). Similar results were obtained based on the symmetric vibrations. These results are in agreement with the notion that the diastereomer penetrates better than K_5L_7 into the LPS acyl chains.

Secondary Structure of the Peptides in LPS Dispersions as Examined by Circular Dichroism Spectroscopy—The secondary structure of the peptides (25 μM) was determined in LPS dispersions (0.1%, ~0.22 mM). The data revealed a 78% α-helical structure for K_5L_7, characterized by double minima at 208 and 222 nm (Fig. 3). As expected, the estimated helicity was significantly decreased (20%) for 4D- K_5L_7. This is in agreement with

TABLE II
Peptide structures and ATR dichroic analysis of LPS multibilayers as determined by ATR-FTIR spectroscopy

Sample[a]	Structure				$\nu_{antisymmetric}(CH_2)$	
	α-Helix	Random coil	Aggregated strands	Distorted/3_{10}-helix	*R*	*f*
	%	%	%	%		
LPS					1.25	0.37
LPS + K_5L_7	75 ± 3		25 ± 1		1.33	0.30
LPS + 4D-K_5L_7		30 ± 3		70 ± 3	1.39	0.25

[a] A 60:1 lipid/peptide molar ratio was used. The results are the average of three independent repetitions with S.D. value of 10%.

the FTIR experiments. Note that a $\theta_{222}/\theta_{208}$ ratio larger than 1.0 for all L-amino acid peptides characterizes interacting α-helices (54, 72). This ratio equals 1.10 for K_5L_7, indicating its assembly in LPS. In contrast, no helix-helix interaction was observed for the diastereomer as revealed by FTIR (Table II) and SPR (see below).

Peptide Partitioning and Insertion into LPS Bilayers as Determined by SPR—We used SPR to determine the ability of the peptides to bind bacterial LPS in the presence or absence of Mg^{2+}. Despite the complex structure of the LPS molecule, it forms bilayer structures similar to phospholipids (35). The binding sensorgrams of K_5L_7 and 4D-K_5L_7 to LPS bilayers (in Mg^{2+}-free buffer) are shown in Fig. 4, *A* and *B*, respectively. The relationships between the maximal binding response obtained (R_{max}) and the peptide's concentration are also given. Both K_5L_7 (*A*) and 4D-K_5L_7 (*B*) interact with LPS bilayers, with the former exhibiting a cooperative binding. This supports our conclusion that K_5L_7 but not 4D-K_5L_7 aggregates in LPS membranes. The cationic antimicrobial peptide SNAP-29 and the human cathelicidin LL-37, which both contain two LPS binding sites, were also found to bind LPS cooperatively (49). However, this cooperativity was primarily intramolecular (*i.e.* involving the N- and C-terminal LPS-binding sites from the same peptide molecule).

A Two-state Model for the Peptide's Interaction with Membranes—We employed a numerical integration analysis that uses nonlinear analysis to fit an integrated rate equation directly to the sensorgrams (56). When fitting the peptide's sensorgrams globally (using different concentrations of peptide) with the simplest 1:1 Langmuir binding model, a poor fit was obtained ($\chi^2 > 100$), confirming that this model does not represent the lipid binding mechanism of the peptides. However, a significantly improved fit ($\chi^2 < 1$) was obtained by applying numerical integration of the two-state reaction model with the binding sensorgrams. This model describes two steps in the binding process between the peptides and lipids; the first step is the binding of the peptide to the surface, followed by a second step in which the peptide is inserted into the membrane's core (58). A set of peptide sensorgrams with different peptide concentrations was used to estimate the kinetic parameters from which the binding constants were derived. The average values for the binding constants are listed in Table III.

The results can be summarized as follows. (i) The active 4D-K_5L_7 has the highest affinity ($\sim 18 \times 10^4$ M^{-1}) toward LPS bilayers in the absence of Mg^{2+}. However, similar affinities were obtained with *E. coli* LPS bound to the α-helical cationic antimicrobial peptides polyphemusin I and polymyxin B, using the dansyl polymyxin displacement assay (23, 73). Note that the affinity of SMAP-29, which contains two LPS binding sites (49), to *E. coli* LPS is similar to that of 4D-K_5L_7, although the latter lacks any known LPS binding domains. Furthermore, deleting one LPS binding site in SMAP-29 completely abolished LPS binding (49). (ii) Consistent with the observation that peptides generally interact with divalent cation binding sites on LPS, the addition of Mg^{2+} resulted in a marked reduction in the affinity of both peptides to LPS. Furthermore, as expected, this reduction was mainly noted in the first binding step. This is in agreement with previous results obtained with polyphemusins binding to *E. coli* LPS (23). (iii) The higher affinity of 4D-K_5L_7, compared with K_5L_7, is due to the second step, insertion into the membrane core. This is demonstrated by the similar K_1 values obtained for the two peptides but higher K_2 values obtained for 4D-K_5L_7 compared with K_5L_7 (Table III). (iv) In all cases, the contribution of the second step to the overall binding process (K_2, insertion into the oligosaccharide core) was much smaller than the contribution of the first step (K_1, initial binding to the surface). The experiments were repeated three times with an S.D. of 10%.

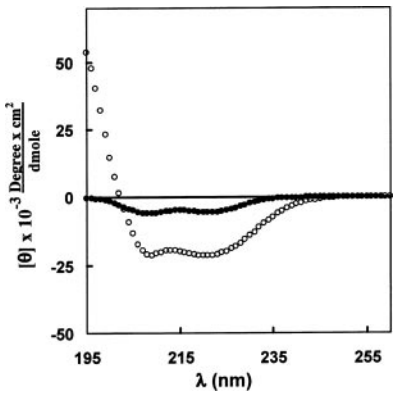

FIG. 3. **CD spectra of K_5L_7 and its 4D-diastereomer.** Spectra were taken at 25 μM peptide dissolved in LPS micelles (0.1%). ●, K_5L_7; ○, 4D-K_5L_7.

Epifluorescence Microscopy—Membranes can be divided into co-existing liquid domains with different compositions. These lipid moieties include unordered and organized bilayer domains. This division process, which is similar to raft formation in cell membranes, has already been observed in GUVs (74, 75). To observe changes in the liquid expanded/liquid condensed domain structures of PE/PG and LPS GUVs, we doped the lipids with 1% Rho-PE and performed epifluorescence microscopy studies (38, 59, 60). For PE/PG GUVs, LE domains were formed (*red areas* in Fig. 5*A*). On the other hand, in the LPS GUVs, there was a marked reduction in the LE domain and the appearance of other structurally different areas, which are LC domains (*dark areas* in Fig. 5*C*). This demonstrates that, compared with PE/PG bilayers, LPS bilayers are generally more condensed and packed and therefore display a large impermeable barrier for the peptides, especially if they aggregate.

The Effect of the Peptides on the Morphology of LPS LUVs Examined by Electron Microscopy—The active 4D-K_5L_7 was added to LPS LUVs at a molar concentration corresponding to an ~50% (3 μM) and ~80% (5 μM) increase in membrane depolarization (based on Fig. 1*B*). The inactive K_5L_7 was added to LPS LUVs at 10 μM, which is 2-fold higher than 4D-K_5L_7. After incubation for 30 min, a drop from a sample was removed, fixed, and examined using transmission electron microscopy. Interestingly, 4D-K_5L_7 caused micellization and a decrease in

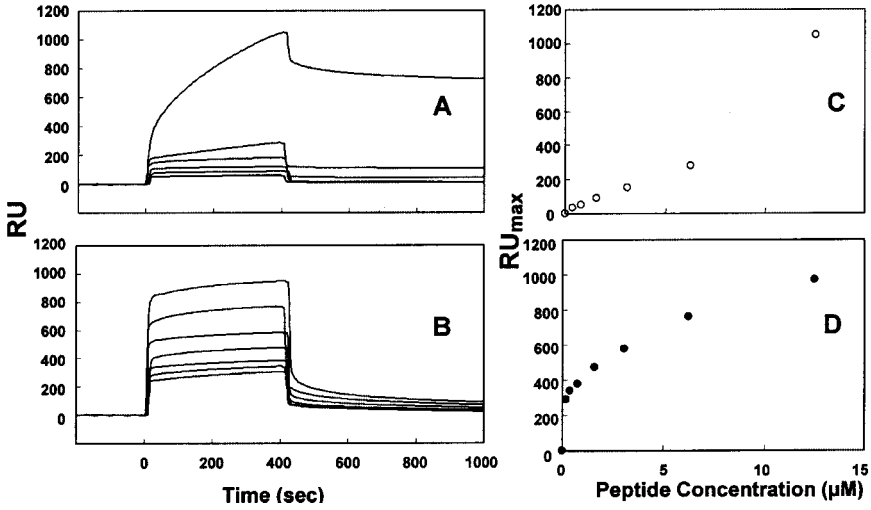

FIG. 4. **Sensograms of the binding of K_5L_7 (*A*) and 4D-K_5L_7 (*B*) peptides to LPS lipid bilayers.** The concentrations of the peptides from *bottom* to the *top* are 0.39, 0.78, 1.56, 3.125, 6.25, and 12.5 μM (in Mg^{2+}-free buffer). *C* and *D*, the corresponding relationships between the maximal binding response (RU_{max}) and the peptide's concentrations. ●, K_5L_7; ○, 4D-K_5L_7.

TABLE III

The binding constants of the peptides to LPS bilayers (immobilized onto an L1 chip), determined by numerical integration using the BIAcore two-step reaction model

The affinity constants, K_1 and K_2, are for the first (binding) and second (insertion) steps, respectively, and the total affinity constant (K) is $K_1 \times K_2$. The results are the average of three independent repetitions with an S.D. of 10%.

Peptides	K_1	K_2	K
		$\times 10^4\ M^{-1}$	
K_5L_7			
Without Mg^{2+}	0.83	10	8.30
With Mg^{2+}	0.12	9.0	1.08
4D-K_5L_7			
Without Mg^{2+}	0.92	20	18.4
With Mg^{2+}	0.08	15	1.20

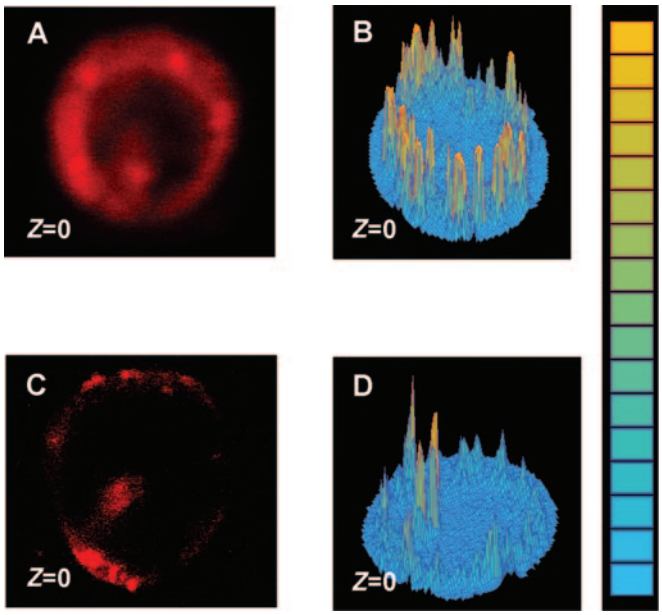

FIG. 5. **Epifluorescence micrographs of GUVs containing PE/PG/PE-Rho (7/3/0.1, w/w/w) (*A* and *B*) and LPS/PE-Rho (10/0.1, w/w) (*C* and *D*).** Liquid expended domains appear in *red*, and LC domains are marked as *dark regions*. *Left panels* show GUV slices in their $Z = 0$, and *right panels* show the relative intensities of the PE-Rho when $Z = 0$. *Bar*, 2 μm.

the size of the vesicles (Fig. 6, *C* and *D*). In contrast, K_5L_7 did not damage the vesicles at all (Fig. 6*B*) in comparison with the untreated control (Fig. 6*A*).

DISCUSSION

The Activity of the Peptides on LPS Reflects Their Potency against Intact Bacteria—This study increases our knowledge regarding the molecular mechanism by which LPS, although it is highly negatively charged and considered as the first target for cationic antimicrobial peptides, can also serve as a barrier to prevent the insertion of peptides into the inner phospholipid membrane. In line with this, we found that the all-L-aa peptide, K_5L_7, was practically inactive against bacteria, although it is highly active in depolarizing phospholipid membranes. The increased ability of this peptide and its 4D-diastereomer to depolarize PE/PG can partially explain why these peptides are similarly active toward bacterial spheroplasts (that lack outer membrane) (Fig. 1, *A* and *C*, respectively) but cannot explain their different activities toward intact bacteria. However, we found a direct correlation between biological activity and the ability to permeate LPS (Fig. 1, *B* and *D*, respectively). Differences in activities against PE/PG, compared with LPS, may result from structural and packing differences between these two lipids. Indeed, epifluorescence micrographs using lipid GUVs showed a significant difference in the domain formation between PE/PG and LPS, particularly changes in the size of the LC and the LE domains. This change could result from intermolecular saccharide-saccharide interactions, not found in typical phospholipids, making LPS molecules tightly associated (32, 33, 40). This unusual tight packing is probably the reason for the decreased ability of the aggregated K_5L_7 (based on FTIR, CD, and SPR experiments) to traverse into the cytoplasmic membrane. A similar argument was proposed for the reduced activity of melittin toward LPS and PC/cholesterol, based on membrane binding and leakage experiments (36).

LPS Binding and Permeation Are Governed by the Amphipathicity and Aggregational States of the Peptides—The structural data can further explain the different biological activities of K_5L_7 and its diastereomer. Both peptides are unstructured in solution (data not shown) but adopt different structures when bound to LPS dispersions (Figs. 2 and 3). Nevertheless, both bind strongly to LPS bilayers, as revealed by using SPR, indicating that structural alterations within the same peptide do not interfere with LPS binding. Note that their affinities for LPS ($\sim 18 \times 10^4\ M^{-1}$) are similar to those of other α-helical cationic antimicrobial peptides (76). However, K_5L_7 and its diastereomer have different modes of interactions; K_5L_7 aggregates and binds in a positive cooperative manner, whereas 4D-K_5L_7 does not (Fig. 4, *C* and *D*).

The affinities of the K_5L_7 and its diastereomer for LPS also approach the values shown for polymyxin B ($66 \times 10^4\ M^{-1}$), an

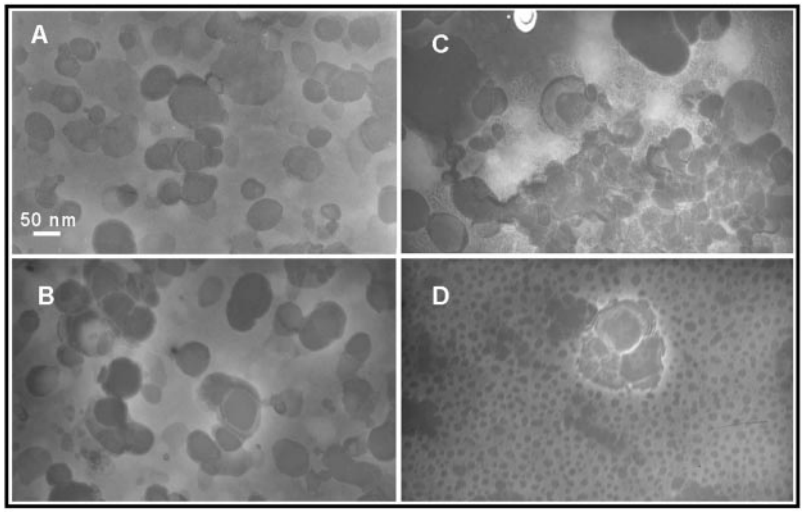

FIG. 6. **Transmission electron micrographs of negatively stained LPS LUVs untreated (*A*) and treated with 10 μM K_5L_7 (*B*).** LPS treated with 3 and 5 μM 4D-K_5L_7 are presented in *C* and *D*, respectively.

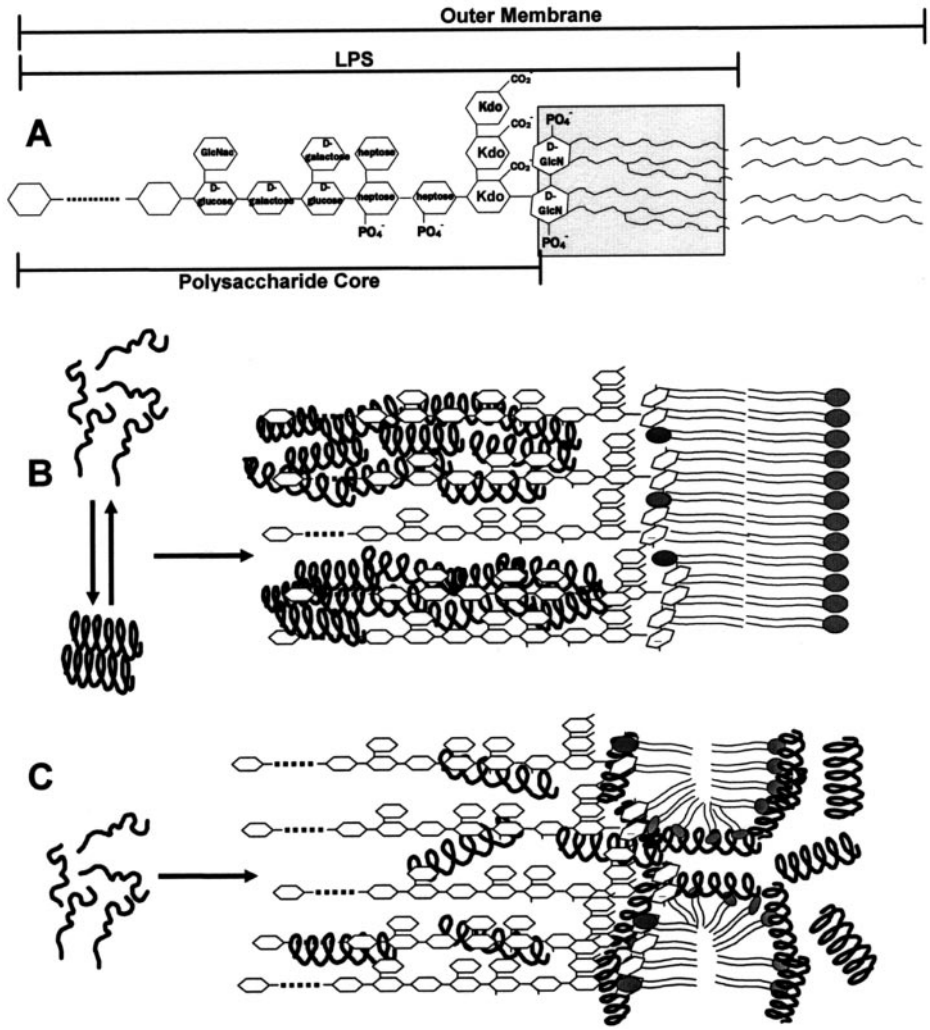

FIG. 7. *A*, schematic structure of Gram-negative outer membrane. *Kdo*, 3-deoxy-D-*manno*-oct-2-ulopyranosonic acid; *P*, phosphate. *B*, schematic representation of mode of binding of the K_5L_7 peptide with LPS. The peptide binds first predominantly by electrostatic interactions to the LPS, self-associates, and cannot traverse into the lipid core. *C*, schematic representation of the possible mechanism of membrane lysis by the 4D-K_5L_7 peptide. The peptide binds first predominantly by electrostatic interactions to the LPS and stays as monomers. The peptide then accumulates on the surface of the lipidic core until a threshold concentration is reached, followed by LPS micellization.

antiseptic cyclic cationic acylated decapeptide (73, 77). Using fluorescence studies, it has been shown that polymyxin B also recognizes LPS in a biphasic manner, corresponding to a rapid initial association followed by a slower insertion (77). The findings that K_5L_7 has significantly reduced LPS-permeating activity but has relatively high LPS binding capacity demonstrate that binding and permeation, although consecutive, are governed by two different molecular mechanisms and are influenced by different peptide parameters. Whereas a nonaggregated conformation is preferred for membrane-permeating activity, LPS binding seems to be independent of the oligomeric state of the molecule.

The Diastereomer but Not the All-L-peptide Traverses the Polysaccharide Core of LPS—The results of the ATR-FTIR spectroscopy, showing surface localization for K_5L_7 further support the notion that the peptide cannot traverse through

the hydrophobic core of LPS. Regarding 4D-K_5L_7, it perturbs both the hydrophilic polysaccharide (head group) region and the hydrophobic lipid core of LPS (Table II). This conclusion is further supported by the different effects of the peptides on the two phosphate groups of the LPS molecules (Fig. 2*C*). On the basis of their different degrees of hydration (78), the two phosphate vibrational bands, at wave number 1224 cm^{-1} and at wave number 1260 cm^{-1}, originate mainly from the more hydrated 1′-phosphate (facing the aqueous phase) and the less hydrated 4′-phosphate (facing the lipidic phase), respectively (40). We found that the peptides interact differently with these two phosphates; 4D-K_5L_7 interacts similarly with the two phosphates, but K_5L_7 interacts only with the more hydrated 1′-phosphate (Fig. 2*C*). These observations indicate that 4D-K_5L_7 penetrates deeper than K_5L_7 into LPS. Thus, it seems reasonable to assume that the LPS polysaccharide core (including its 3-deoxy-D-*manno*-oct-2-ulopyranosonic acid (*Kdo*) moiety) (Fig. 7) prevents the oligomeric (and therefore bulky) K_5L_7 from reaching the lipid core.

The Diastereomeric Peptide Depolarizes and Micellizes the Bacterial Outer Membrane as Part of Its Lytic Mechanism—LPS molecules normally occupy up to 90% of the outer leaflet of the outer membrane and are connected by the Mg^{2+} ions to form an oriented and highly ordered structure (see epifluorescence results (Fig. 5)) (30, 32). We further explored the process of peptide permeation into LPS, which is still controversial (23, 36–38). The initial binding of the hydrophilic face of the diastereomer to the LPS molecules probably involves the displacement of the Mg^{2+} ions (SPR results), followed by increased mobility and disordered packing of the polysaccharide region and acyl chains in LPS. Because the diastereomer molecules are significantly larger than the Mg^{2+} ions that they replace, their insertion into the outer LPS leaflet (Fig. 7) would cause its expansion (FTIR results) as well as "loosening" and depolarization. This might be the reason for the micellization of the LPS vesicles (Fig. 6*D*, *TEM images*). This type of activity, which results in transient "cracks" in the outer membrane, permits the passage of a variety of molecules, including the uptake of the peptide itself. This process, which is referred to as the "self-promoted uptake" pathway (79), may also be explained by the "carpet-like" model of action proposed for many antimicrobial peptides (7, 11, 22, 41, 80–83). This mechanism was recently visualized for the action of the antimicrobial peptide PGLa on intact bacteria by using atomic force microscopy, showing a loosening of the bacterial outer membrane and the formation of micelles originating from disrupted LPS (84).

In summary, this study shed light on several steps regarding the mechanism by which LPS protects Gram-negative bacteria from the action of potent membrane-active antimicrobial peptides (Fig. 7). The investigation of two peptides with the same amino acid composition but with different structures and hydrophobicities enabled better understanding of the specific roles of the helicity, hydrophobicity, and aggregation states of the peptide in LPS binding and permeation. Binding of the peptides to LPS triggers their oligomerization, consequently forming a bulky compound unable to insert into the target's cytoplasmic membrane (Fig. 7*B*). Importantly, the incorporation of D-amino acids can overcome this mechanism by preventing the formation of oligomers and therefore allows the peptide to traverse through the lipid core of LPS (Fig. 7*C*). An interesting example suggesting that native antimicrobial peptides use a similar mechanism to overcome resistance by LPS is presented by bombinins H2 and H4, 20-residue naturally occurring cationic antimicrobial peptides (85). They differ from each other only by the D-configuration of the second amino acid in H4, as a consequence of post-translational modifications (85). Although the reason is not yet known, bombinin H4, similar to D-K_5L_7, is more potent than bombinin H2 toward Gram-negative bacteria (86).

Overall, in addition to increasing our understanding of the molecular basis of the protection of bacteria by LPS, this study presents a potential strategy to overcome resistance by LPS, and it should help in the design of antimicrobial peptides for future therapeutic purposes.

Acknowledgments—We thank V. Kiss for technical assistance in the confocal microscopy studies, Dr. Y. Marikovsky for technical support in the transmission electron microscopy studies, and Dr. A. Rabinkov for assistance in the BIAcore studies.

REFERENCES

1. Boman, H. G. (1995) *Annu. Rev. Immunol.* **13,** 61–92
2. Lehrer, R. I., and Ganz, T. (1999) *Curr. Opin. Immunol.* **11,** 23–27
3. Hancock, R. E., and Diamond, G. (2000) *Trends Microbiol.* **8,** 402–410
4. Hoffmann, J. A., Kafatos, F. C., Janeway, C. A., and Ezekowitz, R. A. (1999) *Science* **284,** 1313–1318
5. Nicolas, P., and Mor, A. (1995) *Annu. Rev. Microbiol.* **49,** 277–304
6. Zasloff, M. (2002) *Nature* **415,** 389–395
7. Hancock, R. E., and Rozek, A. (2002) *FEMS Microbiol. Lett.* **206,** 143–149
8. Epand, R. F., Lehrer, R. I., Waring, A., Wang, W., Maget-Dana, R., Lelievre, D., and Epand, R. M. (2003) *Biopolymers* **71,** 2–16
9. Wieprecht, T., Apostolov, O., Beyermann, M., and Seelig, J. (2000) *Biochemistry* **39,** 15297–15305
10. Matsuzaki, K., Sugishita, K., Harada, M., Fujii, N., and Miyajima, K. (1997) *Biochim. Biophys. Acta* **1327,** 119–130
11. Shai, Y. (1999) *Biochim. Biophys. Acta* **1462,** 55–70
12. Epand, R. M., and Vogel, H. J. (1999) *Biochim. Biophys. Acta* **1462,** 11–28
13. Matsuzaki, K. (1999) *Biochim. Biophys. Acta* **1462,** 1–10
14. Tossi, A., Sandri, L., and Giangaspero, A. (2000) *Biopolymers* **55,** 4–30
15. Dathe, M., and Wieprecht, T. (1999) *Biochim. Biophys. Acta* **1462,** 71–87
16. Steiner, H., Hultmark, D., Engstrom, A., Bennich, H., and Boman, H. G. (1981) *Nature* **292,** 246–248
17. Zasloff, M. (1987) *Proc. Natl. Acad. Sci. U. S. A.* **84,** 5449–5453
18. Mor, A., Nguyen, V. H., Delfour, A., Migliore, S. D., and Nicolas, P. (1991) *Biochemistry* **30,** 8824–8830
19. Zanetti, M., Gennaro, R., Skerlavaj, B., Tomasinsig, L., and Circo, R. (2002) *Curr. Pharm. Des.* **8,** 779–793
20. Mangoni, M. L., Rinaldi, A. C., Di Giulio, A., Mignogna, G., Bozzi, A., Barra, D., and Simmaco, M. (2000) *Eur. J. Biochem.* **267,** 1447–1454
21. Lehrer, R. I., and Ganz, T. (2002) *Curr. Opin. Hematol.* **9,** 18–22
22. Papo, N., and Shai, Y. (2003) *Peptides* **24,** 1693–1703
23. Zhang, L., Scott, M. G., Yan, H., Mayer, L. D., and Hancock, R. E. (2000) *Biochemistry* **39,** 14504–14514
24. Nikaido, H. (1994) *Science* **264,** 382–388
25. Papo, N., Oren, Z., Pag, U., Sahl, H. G., and Shai, Y. (2002) *J. Biol. Chem.* **277,** 33913–33921
26. Bechinger, B. (1997) *J. Membr. Biol.* **156,** 197–211
27. Chaby, R. (1999) *Drug Discov. Today* **4,** 209–221
28. Bechinger, B. (1999) *Biochim. Biophys. Acta* **1462,** 157–183
29. Boman, H. G. (2000) *Immunol. Rev.* **173,** 5–16
30. Chapple, D. S., Hussain, R., Joannou, C. L., Hancock, R. E., Odell, E., Evans, R. W., and Siligardi, G. (2004) *Antimicrob. Agents Chemother.* **48,** 2190–2198
31. Farnaud, S., Spiller, C., Moriarty, L. C., Patel, A., Gant, V., Odell, E. W., and Evans, R. W. (2004) *FEMS Microbiol. Lett.* **233,** 193–199
32. Andra, J., Koch, M. H., Bartels, R., and Brandenburg, K. (2004) *Antimicrob. Agents Chemother.* **48,** 1593–1599
33. Snyder, S., Kim, D., and McIntosh, T. J. (1999) *Biochemistry* **38,** 10758–10767
34. Snyder, D. S., and McIntosh, T. J. (2000) *Biochemistry* **39,** 11777–11787
35. Ding, L., Yang, L., Weiss, T. M., Waring, A. J., Lehrer, R. I., and Huang, H. W. (2003) *Biochemistry* **42,** 12251–12259
36. Allende, D., and McIntosh, T. J. (2003) *Biochemistry* **42,** 1101–1108
37. Hirakura, Y., Kobayashi, S., and Matsuzaki, K. (2002) *Biochim. Biophys. Acta* **3,** 1–2
38. Gutsmann, T., Fix, M., Larrick, J. W., and Wiese, A. (2000) *J. Membr. Biol.* **176,** 223–236
39. Plesiat, P., and Nikaido, H. (1992) *Mol. Microbiol.* **6,** 1323–1333
40. Brandenburg, K., Kusumoto, S., and Seydel, U. (1997) *Biochim. Biophys. Acta* **2,** 183–201
41. Gazit, E., Lee, W. J., Brey, P. T., and Shai, Y. (1994) *Biochemistry* **33,** 10681–10692
42. Moscho, A., Orwar, O., Chiu, D. T., Modi, B. P., and Zare, R. N. (1996) *Proc. Natl. Acad. Sci. U. S. A.* **93,** 11443–11447
43. Sims, P. J., Waggoner, A. S., Wang, C. H., and Hoffmann, J. R. (1974) *Biochemistry* **13,** 3315–3330
44. Loew, L. M., Rosenberg, I., Bridge, M., and Gitler, C. (1983) *Biochemistry* **22,** 837–844
45. Shai, Y., Bach, D., and Yanovsky, A. (1990) *J. Biol. Chem.* **265,** 20202–20209
46. Wu, M., and Hancock, R. E. W. (1999) *J. Biol. Chem.* **274,** 29–35
47. Yanagida, N., Uozumi, T., and Beppu, T. (1986) *J. Bacteriol.* **166,** 937–944
48. Oren, Z., and Shai, Y. (2000) *Biochemistry* **39,** 6103–6114
49. Tack, B. F., Sawai, M. V., Kearney, W. R., Robertson, A. D., Sherman, M. A., Wang, W., Hong, T., Boo, L. M., Wu, H., Waring, A. J., and Lehrer, R. I. (2002) *Eur. J. Biochem.* **269,** 1181–1189
50. Harrick, N. J. (1967) *Internal Reflection Spectroscopy*, John Wiley and Sons,

Inc., New York
51. Ishiguro, R., Kimura, N., and Takahashi, S. (1993) *Biochemistry* **32,** 9792–9797
52. Greenfield, N., and Fasman, G. D. (1969) *Biochemistry* **8,** 4108–4116
53. Wu, C. S., Ikeda, K., and Yang, J. T. (1981) *Biochemistry* **20,** 566–570
54. Meng, F. G., Zeng, X., Hong, Y. K., and Zhou, H. M. (2001) *Biochimie* (*Paris*) **83,** 953–956
55. Albrecht, M. T., Wang, W., Shamova, O., Lehrer, R. I., and Schiller, N. L. (2002) *Respir Res.* **3,** 18
56. Mozsolits, H., Wirth, H. J., Werkmeister, J., and Aguilar, M. I. (2001) *Biochim. Biophys. Acta* **1512,** 64–76
57. Morton, T. A., Myszka, D. G., and Chaiken, I. M. (1995) *Anal. Biochem.* **227,** 176–185
58. Papo, N., and Shai, Y. (2003) *Biochemistry* **42,** 458–466
59. von Tscharner, V., and McConnell, H. M. (1981) *Biophys. J.* **36,** 409–419
60. Weis, R. M. (1991) *Chem. Phys. Lipids* **57,** 227–239
61. Blondelle, S. E., Ostresh, J. M., Houghten, R. A., and Perez, P. E. (1995) *Biophys. J.* **68,** 351–359
62. Verkleij, A. J., Zwaal, R. F., Roelofsen, B., Comfurius, P., Kastelijn, D., and Deenen, L. V. (1973) *Biochim. Biophys. Acta* **323,** 178–193
63. Sawyer, J. G., Martin, N. L., and Hancock, R. E. (1988) *Infect. Immun.* **56,** 693–698
64. Jackson, M., and Mantsch, H. H. (1995) *Crit. Rev. Biochem. Mol. Biol.* **30,** 95–120
65. Frey, S., and Tamm, L. K. (1991) *Biophys. J.* **60,** 922–930
66. Oren, Z., Lerman, J. C., Gudmundsson, G. H., Agerberth, B., and Shai, Y. (1999) *Biochem. J.* **341,** 501–513
67. Hong, J., Oren, Z., and Shai, Y. (1999) *Biochemistry* **38,** 16963–16973
68. Sharon, M., Oren, Z., Shai, Y., and Anglister, J. (1999) *Biochemistry* **38,** 15305–15316
69. Tatulian, S. A., Biltonen, R. L., and Tamm, L. K. (1997) *J. Mol. Biol.* **268,** 809–815
70. Rothschild, K. J., and Clark, N. A. (1979) *Science* **204,** 311–312
71. Dwivedi, A. M., and Krimm, S. (1984) *Biopolymers* **23,** 923–943
72. Monera, O. D., Zhou, N. E., Kay, C. M., and Hodges, R. S. (1993) *J. Biol. Chem.* **268,** 19218–19227
73. Tsubery, H., Ofek, I., Cohen, S., and Fridkin, M. (2000) *Biochemistry* **39,** 11837–11844
74. Dietrich, C., Bagatolli, L. A., Volovyk, Z. N., Thompson, N. L., Levi, M., Jacobson, K., and Gratton, E. (2001) *Biophys. J.* **80,** 1417–1428
75. Baumgart, T., Hess, S. T., and Webb, W. W. (2003) *Nature* **425,** 821–824
76. Zhang, L., Benz, R., and Hancock, R. E. (1999) *Biochemistry* **38,** 8102–8111
77. Thomas, C. J., Surolia, N., and Surolia, A. (1999) *J. Biol. Chem.* **274,** 29624–29627
78. Goormaghtigh, E., Raussens, V., and Ruysschaert, J. M. (1999) *Biochim. Biophys. Acta* **1422,** 105–185
79. Falla, T. J., Karunaratne, D. N., and Hancock, R. E. W. (1996) *J. Biol. Chem.* **271,** 19298–19303
80. Pouny, Y., Rapaport, D., Mor, A., Nicolas, P., and Shai, Y. (1992) *Biochemistry* **31,** 12416–12423
81. Ludtke, S. J., He, K., Heller, W. T., Harroun, T. A., Yang, L., and Huang, H. W. (1996) *Biochemistry* **35,** 13723–13728
82. Matsuzaki, K., Murase, O., and Miyajima, K. (1995) *Biochemistry* **34,** 12553–12559
83. Stark, M., Liu, L. P., and Deber, C. M. (2002) *Antimicrob. Agents Chemother.* **46,** 3585–3590
84. da Silva, A., Jr., and Teschke, O. (2003) *Biochim. Biophys. Acta* **7,** 1–3
85. Mignogna, G., Simmaco, M., Kreil, G., and Barra, D. (1993) *EMBO J.* **12,** 4829–4832
86. Mangoni, M. L., Grovale, N., Giorgi, A., Mignogna, G., Simmaco, M., and Barra, D. (2000) *Peptides* **21,** 1673–1679